

Body-force modelling in thermal compressible flows with lattice Boltzmann method

Zuoxu Li and Xiaowen Shan[†]

Department of Mechanics and Aerospace Engineering, Southern University of Science and Technology, Shenzhen 518055, China

(Received xx; revised xx; accepted xx)

Body force modelling in lattice Boltzmann method (LBM) has been extensively studied in the incompressible limit but rarely discussed for thermal compressible flows. Here we present a systematic approach of incorporating body force in LBM which is valid for thermal compressible and non-equilibrium flows. In particular, a LBM forcing scheme accurate for the energy equation with second-order time accuracy is given. New and essential in this scheme is the third-moment contribution of the force term. It is shown via Chapman-Enskog analysis that the absence of this contribution causes an erroneous heat flux quadratic in Mach number and linear in temperature variation. The theoretical findings are verified and the necessity of the third-moment contribution demonstrated by numerical simulations.

Key words: Lattice Boltzmann method

1. Introduction

Flows involving body forces are widely present in nature and engineering practice. Examples include gravity induced natural convection such as in Rayleigh-Bernard flows, flows in rotating reference system influenced by centrifugal and Coriolis forces, magneto-fluid influenced by electromagnetic force, and many others. In the fast-growing lattice Boltzmann method (LBM), correctly incorporating the body force has an added importance as the body force is also used to model inter-particle interactions giving rise to the rich phenomena of multiphase flows (Shan & Chen 1993; He *et al.* 1998b).

Although the treatment of body force is rather straightforward in both hydrodynamic equations and Boltzmann equation, it remains a non-trivial and sometimes even controversial topic for LBM after a substantial amount of effort and literally a dozen proposed schemes (Mohamad & Kuzmin 2010; Bawazeer *et al.* 2021). The difficulty can be arguably attributed to the fact that LBM was developed from beginning as a discrete kinetic model that was tailored *a posteriori* to exhibit Navier-Stokes-Fourier thermohydrodynamics at the macroscopic level. It lacked a first-principle theory dictating the evolution of the discrete distribution in an external force field. Furthermore, from the perspective of kinetic theory, the configuration-velocity phase space was discretized together, making error analysis complicated.

An early idea was suggested by Shan & Chen (1993) to shift the equilibrium velocity in the collision term to account for the change of momentum which is the leading-order effect of body force. This approach only imposes a condition on the zeroth and first moments of the discrete distribution function. Although reasonably successful in simple flows, subtle issues arose in applications where detailed modeling of the body force effect is required. An example

[†] Email address for correspondence: shanxw@sustech.edu.cn

is the multi-phase fluid where the velocity-shift scheme results in unphysical dependence of the equilibrium densities on the relaxation time (Yu & Fan 2009). Sbragaglia *et al.* (2009) eliminated the inaccuracy in energy equation generated by the shifted velocity by also shifting the temperature. Using the method of undetermined coefficients and matching the macroscopic equation out of Chapman-Enskog calculation with the Navier-Stokes equation, Guo *et al.* (2002) gave a scheme to eliminate the discrete lattice effect caused by spatial-temporal discretization, which also removed the unphysical dependency on the relaxation-time when applied to the multiphase model. This line of approaches, see also Buick & Greated (2000); Ladd & Verberg (2001), calls upon *a posteriori* matching with the hydrodynamic equations and becomes unwieldy when applied to more complicated collision models and higher-order hydrodynamic approximations.

Another strategy is to start from the body force term of the Boltzmann equation, $\mathbf{g} \cdot \nabla_{\xi} f$. He *et al.* (1998a) approximated f by the Maxwell-Boltzmann equilibrium, $f^{(0)}$, and integrated using the trapezoidal rule to advance one time step. An auxiliary variable was introduced to eliminate the implicitness. Martyts *et al.* (1998) pointed out, by examining the Hermite expansion of the body force, that this approximation is exact up to the second moments. By realizing that $\nabla_{\xi} f^{(0)} = -\nabla_{\mathbf{u}} f^{(0)}$, Kupershtokh (2004) introduced the exact difference method (EDM) to model the effect of the body force as $f^{(0)}(\rho, \mathbf{u} + \mathbf{g}\Delta t) - f^{(0)}(\rho, \mathbf{u})$ which correctly advances a local equilibrium to another one with a shifted velocity. However, effect of the non-equilibrium part of the distribution is ignored all together. In both schemes the spatial-temporal discretization was carefully handled to achieve second-order accuracy.

Despite that the differences, similarities, and accuracies of the existing forcing schemes have been theoretically analysed and numerically examined by a number of authors (Kupershtokh *et al.* 2009; Mohamad & Kuzmin 2010; Huang *et al.* 2011; Silva & Semiao 2012; Li *et al.* 2012), it remains inconclusive as to which scheme is the most accurate because the results often depend on flow conditions such as compressibility and steadiness. Possible origins of the discrepancies include insufficient expansions of the distribution function, the collision term, or the body force term, all resulting in different error terms in the recovered macroscopic equations. More importantly, as the LBM being extended to thermal compressible flows, the existing works mainly focus on the recovery of the mass and momentum equations, whereas, except for a few works (Sbragaglia *et al.* 2009), the body force effect on the energy equation is rarely discussed.

More recently the LBM was re-formulated using kinetic theory in continuum in two separate steps (Shan & He 1998; Shan *et al.* 2006). First, the BGK model equation is projected into a finite-dimensional Hilbert space spanned by the Hermite polynomials. By choosing a set of discrete velocity coordinates that forms a Gauss-Hermite quadrature rule and evaluating the BGK equation at these velocities, one obtains the dynamic equations for a set of discrete distributions in the configuration space which preserve the moments of the continuum distribution function and therefore the hydrodynamics of the BGK equation. Second, the equations for the discrete distribution are further discretized in space and time to yield the lattice Boltzmann equation. With the velocity-space discretization of the body force term simply amounted to expanding it in Hermite polynomials, Li *et al.* (2022) showed that by using second-order time integration on the second-order Hermite expansion of the body force term, one can recover *a priori* the force scheme of Guo *et al.* (2002). Moreover, the methodology is generic so that it can be applied to higher-order moment expansions which give rise to the thermal and non-equilibrium dynamics.

In this paper we present a systematic discretization scheme for the body force term which is second-order in space and time, and valid for moments of arbitrary orders. In particular, force terms pertinent to the energy equation are explicitly given, and errors in heat flux caused by insufficient expansion of the force term is also obtained *via* Chapman-Enskog analysis. Numerical verifications were carried out to show that the third-moment contribution in the force term has a non-negligible effect in flows with strong temperature variation. The remainder of the

paper is organized as follows. In Section 2, we present the methodology to systematically obtain the force term in LBM. The third-order expansion of the form term is obtained and its necessity in the energy equation is demonstrated in Chapman-Enskog analysis. In Section 3, we present numerical verifications and analyses. Some further discussions are given in Section 4,

2. Moment expansion of the force term

We first briefly recap the kinetic theoretic formulation of the LBM. Start with the Boltzmann equation with the BGK collision operator

$$\frac{\partial f}{\partial t} + \boldsymbol{\xi} \cdot \nabla f + \mathbf{g} \cdot \nabla_{\boldsymbol{\xi}} f = \Omega(f) = -\frac{1}{\tau} [f - f^{(0)}], \quad (2.1)$$

where \mathbf{x} and $\boldsymbol{\xi}$ are respectively the coordinates in physical and velocity spaces, t the time, $f(\mathbf{x}, \boldsymbol{\xi}, t)$ the single-particle distribution function, \mathbf{g} the acceleration of the body force, $\nabla_{\boldsymbol{\xi}}$ the gradient in velocity space, Ω the collision term, τ the relaxation time, and $f^{(0)}$ the Maxwell-Boltzmann equilibrium distribution function:

$$f^{(0)} = \frac{\rho}{(2\pi)^{D/2}} \exp\left[-\frac{c^2}{2\theta}\right], \quad (2.2)$$

where D is the space dimensionality, $\mathbf{c} = \boldsymbol{\xi} - \mathbf{u}$ and $c^2 = \mathbf{c} \cdot \mathbf{c}$. The fluid density, ρ , velocity, \mathbf{u} , and temperature, θ , are velocity moments of the distribution function

$$\{\rho, \rho \mathbf{u}, D\rho\theta\} = \int f \{1, \boldsymbol{\xi}, c^2\} d\boldsymbol{\xi}. \quad (2.3)$$

The LBM can be formulated as a velocity-space discretization by first projecting Eq. (2.1) into a finite-dimensional functional space spanned by Hermite polynomials and then evaluating at discrete velocities that form a Gauss-Hermite quadrature rule in the velocity space (Grad 1949; Shan & He 1998; Shan *et al.* 2006). The latter requirement ensures that the leading velocity moments are exactly preserved by the discrete distribution function values. A key step in this formulation is to expand all terms in Eq. (2.1) into finite Hermite series. Assuming f has the following expansion in the laboratory reference frame

$$f_N(\mathbf{x}, \boldsymbol{\xi}, t) = \omega(\boldsymbol{\xi}) \sum_{n=0}^N \frac{1}{n!} \mathbf{a}^{(n)}(\mathbf{x}, t) : \mathcal{H}^{(n)}(\boldsymbol{\xi}), \quad (2.4)$$

where, N is the expansion order, ‘:’ stands for full contraction between two tensors, and $\mathbf{a}^{(n)}(\mathbf{x}, t)$ the expansion coefficients given by

$$\mathbf{a}^{(n)}(\mathbf{x}, t) = \int f_N(\mathbf{x}, \boldsymbol{\xi}, t) \mathcal{H}^{(n)}(\boldsymbol{\xi}) d\boldsymbol{\xi}. \quad (2.5)$$

The corresponding expansion of the body-force term was given by Martys *et al.* (1998) as

$$F(\boldsymbol{\xi}) \equiv -\mathbf{g} \cdot \nabla_{\boldsymbol{\xi}} f_N = \omega(\boldsymbol{\xi}) \sum_{n=1}^{N+1} \frac{1}{n!} n \mathbf{g} \mathbf{a}^{(n-1)} : \mathcal{H}^{(n)}(\boldsymbol{\xi}), \quad (2.6)$$

where $\mathbf{g} \mathbf{a}^{(n-1)}$ is a rank- n symmetric tensor denoting the *symmetric product* between \mathbf{g} and $\mathbf{a}^{(n-1)}$. Noticing that $\mathbf{a}^{(0)} = \rho$ and $\mathbf{a}^{(1)} = \rho \mathbf{u}$, the first two terms in Eq. (2.6) can be evaluated as

$$F(\boldsymbol{\xi}) \cong \omega \rho [\mathbf{g} \cdot \boldsymbol{\xi} + (\mathbf{g} \cdot \boldsymbol{\xi})(\mathbf{u} \cdot \boldsymbol{\xi}) - \mathbf{g} \cdot \mathbf{u}]. \quad (2.7)$$

We note that most existing force schemes are based on the expression above (Li *et al.* 2022). To extend the body force to higher moments, the higher terms can be calculated using Eq. (2.5), *e.g.*

$$\mathbf{a}^{(2)} = \int f_N (\boldsymbol{\xi}^2 - \boldsymbol{\delta}) d\boldsymbol{\xi} = \rho (\mathbf{u}^2 - \boldsymbol{\delta}) + \int f_N c c d\boldsymbol{\xi}. \quad (2.8)$$

The last term is the *momentum flux density* tensor which can be decomposed into the *normal pressure*, $\rho\boldsymbol{\delta}$, and the traceless *deviatoric stress* tensor, $\boldsymbol{\sigma}$, as

$$\int f_N c c d\boldsymbol{\xi} = \rho\boldsymbol{\delta} - \boldsymbol{\sigma}. \quad (2.9)$$

Comparing with the Hermite expansion of $f^{(0)}$, we recognize that

$$\mathbf{a}^{(2)} = \mathbf{a}_0^{(2)} - \boldsymbol{\sigma}, \quad (2.10)$$

where $\mathbf{a}_0^{(n)}$ denotes the Hermite coefficients of $f^{(0)}$. Using $\mathcal{H}^{(3)} = \boldsymbol{\xi}^3 - 3\boldsymbol{\xi}\boldsymbol{\delta}$, the third-order term can be obtained as

$$\begin{aligned} \mathbf{g}\mathbf{a}^{(2)} : \mathcal{H}^{(3)} &= \rho \{ (\mathbf{g} \cdot \boldsymbol{\xi}) [(\mathbf{u} \cdot \boldsymbol{\xi})^2 - u^2 + (\theta - 1)(\boldsymbol{\xi}^2 - D - 2)] - 2(\mathbf{g} \cdot \mathbf{u})(\mathbf{u} \cdot \boldsymbol{\xi}) \} \\ &\quad - (\mathbf{g} \cdot \boldsymbol{\xi})\boldsymbol{\sigma} : \boldsymbol{\xi}\boldsymbol{\xi} + 2\boldsymbol{\sigma} : \mathbf{g}\boldsymbol{\xi}. \end{aligned} \quad (2.11)$$

Two remarks can be made here. First, the first term on the *r.h.s.* is the contribution of $\mathbf{a}_0^{(2)}$ and is proportional to u^2 or $\theta - 1$. The terms proportional to $\boldsymbol{\sigma}$ are the contributions of the non-equilibrium part of the distribution. Secondly, the body force generates momentum and total kinetic energy in the form of bulk fluid motion, but does not generate any heat as can be seen from its heat production rate

$$\int (\mathbf{g} \cdot \nabla_{\boldsymbol{\xi}} f) c^2 d\boldsymbol{\xi} = \mathbf{g} \cdot \int c^2 \nabla_{\boldsymbol{\xi}} f d\boldsymbol{\xi}. \quad (2.12)$$

Integrating by part and noticing that as $\boldsymbol{\xi} \rightarrow \infty$, f vanishes faster than any power of $\boldsymbol{\xi}$, we have

$$\int c^2 \nabla_{\boldsymbol{\xi}} f d\boldsymbol{\xi} = - \int f \nabla_{\boldsymbol{\xi}} c^2 d\boldsymbol{\xi} = -2 \int f (\boldsymbol{\xi} - \mathbf{u}) d\boldsymbol{\xi} = 0. \quad (2.13)$$

Note that for the truncated f_N , the above equalities hold if and only if $N \geq 2$.

Once restricted in the finite-dimensional Hermite space, Eq. (2.1) can be further discretized to yield the lattice Boltzmann equations (Shan *et al.* 2006). Let w_i and $\boldsymbol{\xi}_i$, $i \in \{1, \dots, d\}$, be the weights and abscissas of a degree- Q Gauss-Hermite quadrature rule, *i.e.* for any polynomial, $p(\boldsymbol{\xi})$, of a degree not exceeding Q , we have

$$\int \omega(\boldsymbol{\xi}) p(\boldsymbol{\xi}) d\boldsymbol{\xi} = \sum_{i=1}^d w_i p(\boldsymbol{\xi}_i). \quad (2.14)$$

For the f_N in Eq. (2.4), f_N/ω is a degree- N polynomial. Provided that $Q \geq 2N$, Eq. (2.5) reduces to a summation

$$\mathbf{a}^{(n)} = \int \omega \left[\frac{f_N}{\omega} \mathcal{H}^{(n)} \right] d\boldsymbol{\xi} = \sum_{i=1}^d f_i \mathcal{H}^{(n)}(\boldsymbol{\xi}_i), \quad \forall n \leq N, \quad (2.15)$$

where f_i is the *discrete distribution* defined as

$$f_i(\mathbf{x}, t) \equiv \frac{w_i f_N(\mathbf{x}, \boldsymbol{\xi}_i, t)}{\omega(\boldsymbol{\xi}_i)}, \quad i \in \{1, \dots, d\}. \quad (2.16)$$

In particular, as special cases of Eq. (2.15), Eqs. (2.3) become

$$\rho = \sum_i f_i, \quad \rho \mathbf{u} = \sum_i f_i \boldsymbol{\xi}_i, \quad \rho (u^2 + D\theta) = \sum_i f_i \boldsymbol{\xi}_i^2. \quad (2.17)$$

The governing equation of f_i can be obtained by evaluating Eq. (2.1) at ξ_i :

$$\frac{\partial f_i}{\partial t} + \xi_i \cdot \nabla f_i = \Omega_i(f) + F_i, \quad i \in \{1, \dots, d\}. \quad (2.18)$$

where $F_i \equiv w_i F(\xi_i)/\omega(\xi_i)$. Combining Eqs. (2.8) and (2.11), the *discrete body force* up to the third moment is

$$F_i = w_i \rho (\mathbf{g} \cdot \xi_i) \left\{ 1 + \mathbf{u} \cdot \xi_i + \frac{1}{2} [(\mathbf{u} \cdot \xi_i)^2 - u^2 + (\theta - 1)(\xi_i^2 - D - 2)] \right\} - w_i \rho (\mathbf{g} \cdot \mathbf{u})(1 + \mathbf{u} \cdot \xi_i) - \frac{w_i}{2} [(\mathbf{g} \cdot \xi_i) \boldsymbol{\sigma} : \xi_i \xi_i - 2 \boldsymbol{\sigma} : \mathbf{g} \xi_i]. \quad (2.19)$$

Further discretizing space and time by integrating Eq. (2.18) using second-order schemes (He *et al.* 1998a; Li *et al.* 2022), we arrive at the lattice Boltzmann equation with body force

$$f_i(\mathbf{x} + \boldsymbol{\xi}, t + 1) - f_i(\mathbf{x}, t) = -\frac{1}{\hat{\tau}} \left[f_i - \overline{f_i^{(0)}} \right] + \left[1 - \frac{1}{2\hat{\tau}} \right] \overline{F}_i, \quad (2.20)$$

where $\hat{\tau} = \tau + 1/2$, $f_i^{(0)} \equiv w_i f_N^{(0)}(\mathbf{x}, \xi_i, t)/\omega(\xi_i)$ with $f_N^{(0)}$ being the finite Hermite expansion of $f^{(0)}$. The over-line stands for evaluation using values of density, velocity and temperature at the mid-point of a time step. Noticing the conservation of mass and heat by both the normal collision operator and the body-force term, these are ρ , $\mathbf{u} + \mathbf{g}/2$ and θ respectively. The deviatoric stress tensor at the mid-point of a time step, $\overline{\boldsymbol{\sigma}}$, can be calculated by

$$\overline{\boldsymbol{\sigma}} = - \left(1 - \frac{1}{2\hat{\tau}} \right) \left\{ \sum_i \left[f_i - \overline{f_i^{(0)}} \right] (\xi_i - \mathbf{u})^2 - \frac{\rho \mathbf{g}^2}{2} \right\}. \quad (2.21)$$

Nevertheless, in the quasi-equilibrium regime where $f - f^{(0)} \ll f^{(0)}$, the above contribution can be neglected all together as demonstrated by numerical verifications and Chapman-Enskog analysis in the later sections. We note that expressions similar to Eq. (2.19) can be obtained for any order of expansion to taking into account higher moments of the distribution function. Particularly, if only the second-moment contribution is retained, Eq. (2.20) is identical to the forcing scheme of Guo *et al.* (2002).

We now analyse the macroscopic effects of the force term by Chapman-Enskog analysis. As shown previously by Shan *et al.* (2006), with the Hermite-expanded distribution function and BGK collision operator, the Chapman-Enskog asymptotic analysis results in recurrent relations among the Hermite coefficients of various orders. Particularly for the first approximations (Navier-Stokes), we have

$$\mathbf{a}_1^{(n)} = -\tau \left[\frac{\partial \mathbf{a}_0^{(n)}}{\partial t} + \nabla \cdot \mathbf{a}_0^{(n+1)} + n \nabla \mathbf{a}_0^{(n-1)} - n \mathbf{g} \mathbf{a}_0^{(n-1)} \right]. \quad (2.22)$$

As it is well-known that the equation above leads to the correct Navier-Stokes-Fourier equations (Huang 1987; Shan *et al.* 2006), the error in the macroscopic equations caused by insufficient expansion of the force term can be analyzed by examining the contributions of the last term on the *r.h.s.*. In most force schemes it is retained up to $n \leq 2$. While accurate for the momentum equation, this causes an error in the third Hermite coefficient of the first correction $\mathbf{a}_1^{(3)} = -3\tau \mathbf{g} \mathbf{a}_0^{(2)}$ which in turn results in the following error in the heat flux

$$\begin{aligned} \mathbf{q}_{err} &= \frac{1}{2} \int f_{err} c^2 c d\xi = \frac{1}{12} \mathbf{a}_1^{(3)} : \int \omega(\xi) \mathcal{H}^{(3)}(\xi) c^2 c d\xi \\ &= -\frac{1}{2} \rho \tau \{ [u^2 + (\theta - 1)(D + 2)] \mathbf{g} + 2(\mathbf{g} \cdot \mathbf{u}) \mathbf{u} \}, \end{aligned} \quad (2.23)$$

which is second-order in u , first-order in $\theta - 1$, and can not be ignored in flows with strong thermal effects. However, the non-equilibrium part in Eq. (2.19), $-3\mathbf{g}\sigma$, contributes to the heat flux as

$$\mathbf{q}_{err} = \frac{1}{2}\tau\mathbf{g} \cdot \boldsymbol{\sigma} \approx \frac{1}{2}\tau^2 p\mathbf{g} \cdot \left[\nabla\mathbf{u} + (\nabla\mathbf{u})^T - \frac{2}{D}(\nabla \cdot \mathbf{u})\boldsymbol{\delta} \right], \quad (2.24)$$

which is $O(\tau^2)$ and can be omitted in continuum flows but may have significant effect in non-equilibrium ones.

3. Numerical Validation

To verify the above analysis, we conducted two numerical tests, *i.e.*, compressible Poiseuille flow under cross gravity and heat transfer between two concentric cylinders under centrifugal force. These flows are chosen as the deviatoric stress does not automatically vanish by configuration. In all LBM simulations the equilibrium distribution is expanded to fourth order and the two-dimensional, ninth-order accurate D2Q37 quadrature rule is employed (Shan 2016). Since this model involves discrete velocities of multiple layers, we have developed a multi-speed mass-conserving boundary condition (BC) which will be published elsewhere. For the present purposes the results are insensitive to the implementation of the BC.

3.1. Compressible Poiseuille flow under cross acceleration

Consider a two-dimensional steady laminar flow between two infinite horizontal plates under a homogeneous constant gravity force $\mathbf{g} = (g_x, g_y)$, where x and y are respectively the horizontal and vertical directions. The flow is assumed to be steady and one-dimensional with velocity in the x direction only and all quantities are functions of y . We have therefore $u_y = 0$ and $\partial/\partial x = \partial/\partial t = 0$. The Navier-Stokes-Fourier equations reduce to

$$-\mu \frac{\partial^2 u_x}{\partial y^2} = \rho g_x, \quad \frac{\partial \rho \theta}{\partial y} = \rho g_y, \quad \text{and} \quad \mu \left(\frac{\partial u_x}{\partial y} \right)^2 + \lambda \frac{\partial^2 \theta}{\partial y^2} = 0, \quad (3.1)$$

where ρ , u_x and θ are density, velocity and temperature respectively, μ and λ the dynamic viscosity and heat conductivity, both assumed constant. Dirichlet boundary conditions are imposed for u_x and θ on the bottom and top boundaries at $y = 0$ and H respectively

$$u_x|_{y=0} = U_b, \quad u_x|_{y=H} = U_t, \quad \theta|_{y=0} = \theta_b, \quad \theta|_{y=H} = \theta_t, \quad (3.2)$$

where U_b , U_t and θ_b , θ_t are the tangential velocity and temperature at the bottom and top boundaries respectively. As Eqs. (3.1) are non-trivial to solve analytically, for the reference solution, we utilized a finite-difference scheme which is detailed in Appendix A.

All LBM simulations of compressible Poiseuille flow were performed on a $L_x \times L_y$ lattice where $L_x = 3$ and $L_y = 150$. The channel height is thus $H = L_y c$ where $c \approx 1.19698$ is the lattice constant of D2Q37 (Shan 2016). The velocity at both walls were set at $U_t = U_b = 0$. To investigate the effect of temperature gradient, two simulations were performed for $\theta_b = 1.0$, $\theta_t = 1.1$ and $\theta_b = 0.7$, $\theta_t = 1.4$, corresponding to a total cross-channel temperature variation of 10% and 100% respectively. Define $U_c = \rho_0 g_x H^2 / 8\mu$ which is the velocity (and also the Mach number *w.r.t.* the isothermal speed of sound) at the centre of channel when both ρ and θ are homogeneous. The corresponding Reynolds number is $Re = \rho_0 U_c H / \mu$ where ρ_0 is the averaged density. Setting $U_c = 1.5$, $Re = 1800$ and $\rho_0 = 1$, the other parameters are determined as: $g_x = U_c^2 / ReH$, $\mu = \rho_0 U_c H / Re$ and $\lambda = c_p \mu / Pr$, where the Prandtl number $Pr = 1$ for BGK collision term, and the isobaric heat capacity $c_p = (D + 2)/2$. To maintain both μ and λ as homogeneous constants, the relaxation time was set to $\tau = \mu / \rho \theta$. The cross-flow gravity, g_y , points downward and was set so that $g_y / g_x = -50$.

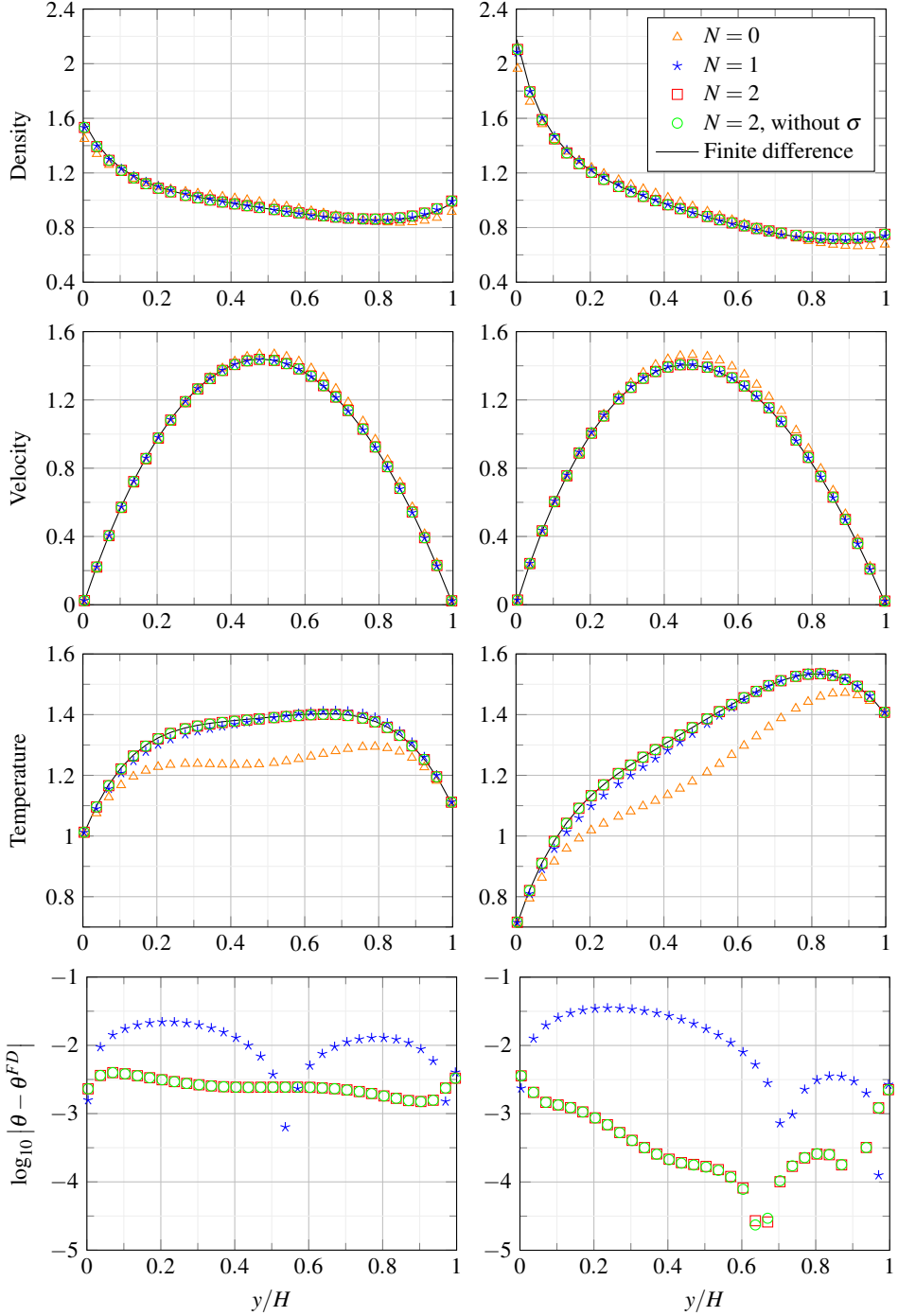


Figure 1: Compressible Poiseuille flow with cross-flow gravity and heat gradient. Shown from top to bottom are profiles of density, velocity, temperature, and errors in temperature as computed by the force term expanded to orders corresponding to $N = 0, 1$ and 2 in Eq. (2.6). The reference is a high-precision finite-difference solution which is also shown. In the left column are the results for $\theta_b = 1.0$, $\theta_t = 1.1$, corresponding to a 10% total temperature variation, and in the right column are those for $\theta_b = 0.7$, $\theta_t = 1.4$, corresponding to a 100% total temperature variation.

Shown in Figs. 1 are the profiles of density, velocity, temperature, and errors in temperature for the two sets of simulations with different temperature variations. To demonstrate the effects of the various moments in the force term, simulations were performed with the force term expanded to three different orders, corresponding to $N = 0, 1,$ and 2 in Eq. (2.6). In addition, the cases of $N = 2$ were run with and without the contributions of σ in Eq. (2.19). As the reference solution, a high-resolution ($N = 450$) finite-difference results are also shown. We first note that due to the presence of cross-flow gravity and temperature gradient, the density and temperature are asymmetric *w.r.t.* to the centre line. The velocity peak is also less than U_c and does not occur at the centre. These effects are stronger in the cases with larger temperature variation.

Consistent with the theoretical analysis that the second-order ($N = 1$) force term is necessary in recovering the momentum equation and conservation of internal energy, it is evident from simulation results that retaining only the first-order force term ($N = 0$) causes significant overall discrepancies. The more common second-order ($N = 1$) approximation yields satisfactory results for density and velocity, in accordance with the theoretical prediction of Eq. (2.22). However, noticeable differences between the second-order and reference solutions appear in the temperature profile and are more pronounced in the high temperature-variation cases. This discrepancy is eliminated in the third-order ($N = 2$) solutions, confirming the correctness and necessity of the third-order contribution by Eq. (2.19). Moreover, the contribution of the deviatoric tensor to the force term appears to be negligible in all cases tested, confirming the Chapman-Enskog analysis in the previous section.

3.2. Heat transfer between concentric cylinders under centrifugal force

The second test is the two-dimensional heat transfer between two concentric cylinders maintained at different temperatures and rotating with the same angular speed, α . In the rotating reference frame, the fluid is assumed static and subject to the centripetal acceleration of $\alpha^2 R$ where R is the radial coordinate. The Navier-Stokes-Fourier equations have the following one-dimensional solution

$$\theta = \theta_i + (\theta_o - \theta_i) \frac{\ln R/R_i}{\ln R_o/R_i}, \quad \text{and} \quad \rho = \frac{\rho_i \theta_i}{\theta} \exp \left[\int_{R_i}^R \frac{\alpha^2 r}{\theta(r)} dr \right], \quad (3.3)$$

where ρ, θ are density and temperature respectively, the subscripts i and o denote values at the inner and outer cylinders. The reference solution of density is solved by a high-precision numerical integration. Required the average of density $\bar{\rho} = \rho_o$, the ρ_i is obtained by integrating the density in the whole domain.

The LBM simulations were performed on a $L \times L$ lattice where $L = 250$. The radial centripetal acceleration is $-\alpha^2 R$. The radius ratio R_o/R_i is set to 5 with $R_o = Lc/2$. Using the width of the annular, $R_o - R_i$, as the characteristic length and the centre-line velocity, $U_c \equiv \alpha(R_o + R_i)/2$, as the characteristic speed, the Reynolds number is defined as $Re = \rho_o \alpha (R_o^2 - R_i^2) / 2\mu$ where μ is the dynamic viscosity. As in the previous case, the relaxation time is set to $\tau = \mu / \rho \theta$ so that μ is a constant. Note that the fluid is static, and the centre-line velocity, U_c , measures the compressibility as the isothermal Mach number, and the Reynolds number only plays the role of a dimensionless viscosity. As there is no flow in the rotating frame, all quantities are insensitive to the Reynolds number.

Shown in Figs. 2 are the radial profiles of density, temperature and the associated errors as computed with the force term expanded to various orders. The parameters are: $Re = 100, U_c = 0.3,$ and $\rho_o = 1$. Two simulations were performed for $\theta_i = 1, \theta_o = 1.1,$ and for $\theta_i = 1.4, \theta_o = 0.7$. Note that the first and second expansions are identical as $\mathbf{u} = 0$ in this case. To be seen is that if the third-moment contribution is omitted, the errors in temperature profile is significant especially in the larger temperature variation case. It is also evident from the results that the third-order

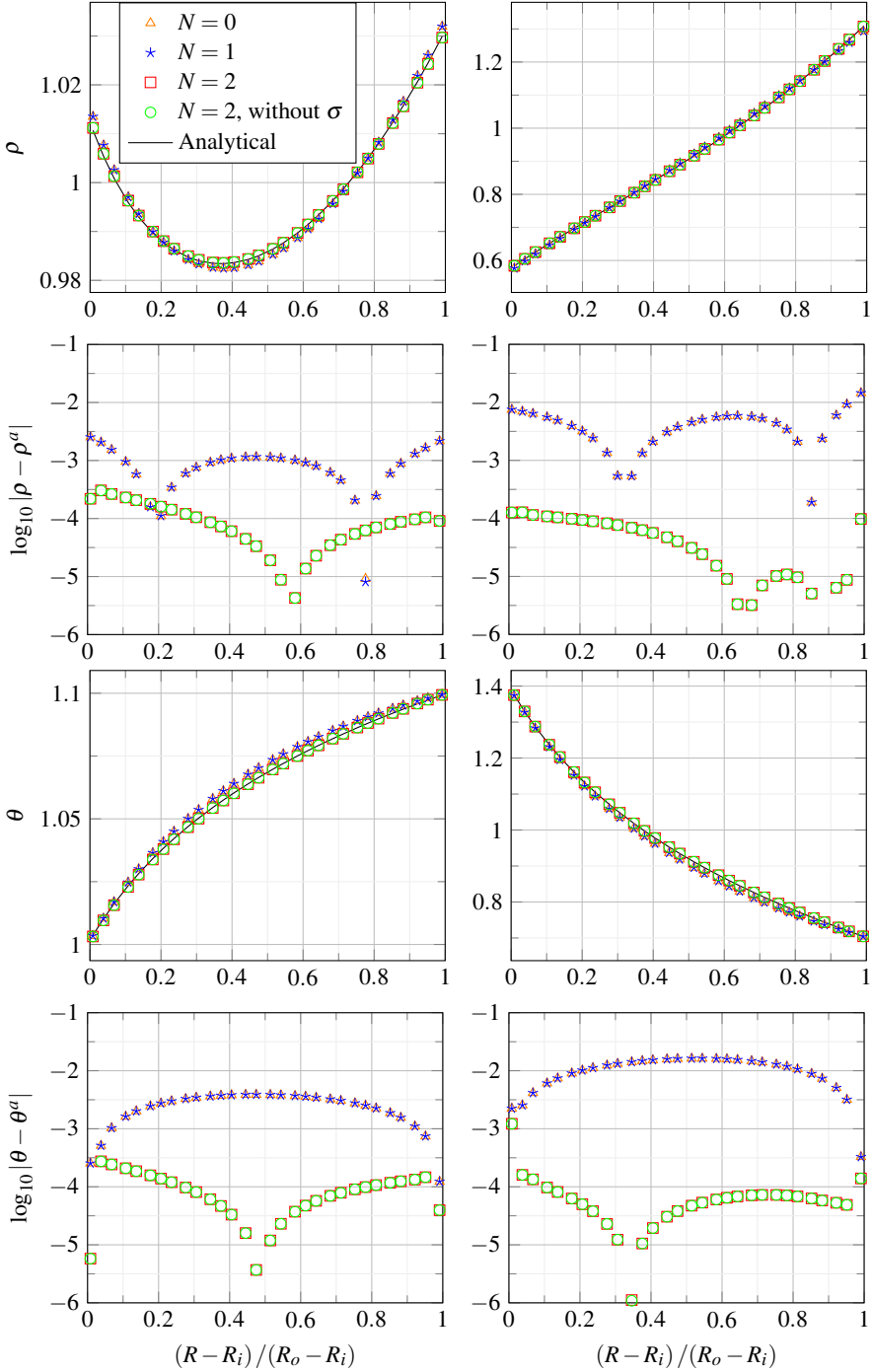


Figure 2: Heat conduction between two rotating concentric cylinders. Shown are the radial profiles of density and temperature and the associated errors computed with the force terms expanded to various orders. The superscript a denotes the analytical solutions. The left column shows the result for $\theta_i = 1$, $\theta_o = 1.1$, and the right column shows the result for $\theta_i = 1.4$, $\theta_o = 0.7$.

contribution is necessary to correctly recover the energy equation. The contribution of the stress tensor, σ , vanishes as σ itself vanishes in absence of fluid flow.

4. Conclusion

In summary, we gave a generic approach of incorporating body force in lattice Boltzmann method based on the Hermite expansion of the force term in the Boltzmann equation. In particular, a novel LBM forcing scheme for thermal compressible flows with second-order time accuracy is obtained which includes the third-order contribution of the force term. The errors caused by the omission of this correction in common practices is identified with an error in heat flux *via* Chapman-Enskog analysis. All theoretical findings, including the correctness and necessity of the new forcing term, are confirmed numerically.

We note that the present approach is independent of neither the form of the equilibrium distribution nor the underlying lattice, and can be straightforwardly extended to include higher moments which are significant in non-equilibrium flows. Although for simplicity, we used the BGK collision model in present work. It is also straightforward to adapt it to more complicated collision models such as the spectral multiple relaxation time model.

Appendix A. Finite-difference solution of compressible Poiseuille flow

We outline the one-dimensional finite-difference solution of the steady, gravity-driven, compressible Poiseuille flow with cross-flow gravity and temperature gradient. Along the channel height the domain is divided into N nodes with $\Delta y = H/(N-1)$. Let ρ_j, u_j, θ_j be the density, velocity and temperature at the j -th node. Applying second-order central difference scheme to the horizontal momentum and energy equations, and first order forward scheme to the vertical momentum equation, Eqs. (3.1) are discretized as:

$$u_{j+1} - 2u_j + u_{j-1} = -\frac{g_x \Delta y^2}{\mu} \rho_j \quad 2 \leq j \leq N-1, \quad (\text{A } 1a)$$

$$\rho_{j+1} \theta_{j+1} - \rho_j \theta_j = \rho_j g_y \Delta y \quad 1 \leq j \leq N-1, \quad (\text{A } 1b)$$

$$\mu (u_{j+1} - u_{j-1})^2 + 4\lambda (\theta_{j+1} - 2\theta_j + \theta_{j-1}) = 0 \quad 2 \leq j \leq N-1. \quad (\text{A } 1c)$$

The Dirichlet boundary condition dictates that

$$u_1 = U_b, \quad u_N = U_t, \quad \theta_1 = \theta_b, \quad \theta_N = \theta_t. \quad (\text{A } 2)$$

The mass conservation yields

$$\left(\frac{\rho_1}{2} + \sum_{j=2}^{N-1} \rho_j + \frac{\rho_N}{2} \right) = \rho_0 (N-1). \quad (\text{A } 3)$$

There are $3N-2$ equations for $3N-2$ unknowns. As the above discretized equations are non-linear and coupled, an iterative method is used where the non-linear term $\mu(u_{j+1} - u_{j-1})^2$ is evaluated using variables at the previous iteration. The equations at iteration t can be written as:

$$u'_{j+1} - 2u'_j + u'_{j-1} + \frac{g_x \Delta y^2}{\mu} \rho'_j = 0, \quad 2 \leq j \leq N-1, \quad (\text{A } 4a)$$

$$\rho'_{j+1} \theta'_{j+1} - \rho'_j (\theta'_j + g_y \Delta y) = 0, \quad 1 \leq j \leq N-1, \quad (\text{A } 4b)$$

$$\mu \left(u'_{j+1} - u'_{j-1} \right)^2 + 4\lambda (\theta'_{j+1} - 2\theta'_j + \theta'_{j-1}) = 0, \quad 2 \leq j \leq N-1, \quad (\text{A } 4c)$$

$$\left(\frac{\rho'_1}{2} + \sum_{j=2}^{N-1} \rho'_j + \frac{\rho'_N}{2} \right) = \rho_0(N-1). \quad (\text{A } 4d)$$

The Eq. (A 4) is a system of linear equations which was solved by the following process. With the initial guess of u chosen as:

$$u = -\frac{g_x}{2\mu} y(y-H) + \frac{U_t - U_b}{H} y + U_b, \quad y \in [0, H]. \quad (\text{A } 5)$$

the temperature field can be solved from Eq. (A 4c). The density field is solved next from Eqs. (A 4b)–(A 4d), followed by solving the velocity field from Eq. (A 4a). This process is iterated until convergence.

Acknowledgment

This work was supported by the National Natural Science Foundation of China Grant 92152107, Dept. of Science and Technology of Guangdong Province Grant 2020B1212030001, and Shenzhen Science and Technology Program Grant KQTD20180411143441009.

Declaration of Interests

The authors report no conflict of interest.

REFERENCES

- BAWAZEER, SALEH A., BAAKEEM, SALEH S. & MOHAMAD, A. A. 2021 A Critical Review of Forcing Schemes in Lattice Boltzmann Method: 1993–2019. *Arch. Comput. Methods Eng.* **28** (7), 4405–4423.
- BUICK, JAMES M & GREATED, C A 2000 Gravity in a lattice Boltzmann model. *Phys. Rev. E* **61** (5), 5307–5320.
- GRAD, HAROLD 1949 On the kinetic theory of rarefied gases. *Commun. Pure Appl. Math.* **2** (4), 331–407.
- GUO, ZHAOLI, ZHENG, CHUGUANG & SHI, BAOCHANG 2002 Discrete lattice effects on the forcing term in the lattice Boltzmann method. *Phys. Rev. E* **65** (4), 046308.
- HE, XIAOYI, CHEN, SHIYI & DOOLEN, GARY D. 1998a A Novel Thermal Model for the Lattice Boltzmann Method in Incompressible Limit. *J. Comput. Phys.* **146** (1), 282–300.
- HE, XIAOYI, SHAN, XIAOWEN & DOOLEN, GARY D. 1998b Discrete Boltzmann equation model for nonideal gases. *Phys. Rev. E* **57** (1), R13–R16.
- HUANG, HAIBO, KRAFczyk, MANFRED & LU, XIYUN 2011 Forcing term in single-phase and Shan-Chen-type multiphase lattice Boltzmann models. *Phys. Rev. E* **84** (4), 046710.
- HUANG, KERSON 1987 *Statistical Mechanics*, 2nd edn. New York: John Wiley & Sons.
- KUPERSHTOKH, ALEXANDER L. 2004 New method of incorporating a body force term into the lattice Boltzmann equation. In *Proceedings 5th Int. EDH Work.*, pp. 241–246. Poitiers.
- KUPERSHTOKH, ALEXANDER L., MEDVEDEV, DMITRY & KARPOV, D.I. 2009 On equations of state in a lattice Boltzmann method. *Comput. Math. with Appl.* **58** (5), 965–974.
- LADD, ANTHONY J. C. & VERBERG, ROLF 2001 Lattice-Boltzmann Simulations of Particle-Fluid Suspensions. *J. Stat. Phys.* **104** (September), 1191–1251.

- LI, Q., LUO, KAI H. & LI, X. J. 2012 Forcing scheme in pseudopotential lattice Boltzmann model for multiphase flows. *Phys. Rev. E* **86** (1), 016709.
- LI, XUHUI, DUAN, WENYANG & SHAN, XIAOWEN 2022 Second-order force scheme for lattice Boltzmann method, arXiv: 2212.07494.
- MARTYS, NICOS S., SHAN, XIAOWEN & CHEN, HUDONG 1998 Evaluation of the external force term in the discrete Boltzmann equation. *Phys. Rev. E* **58** (5), 6855–6857.
- MOHAMAD, A. A. & KUZMIN, ALEXANDR 2010 A critical evaluation of force term in lattice Boltzmann method, natural convection problem. *Int. J. Heat Mass Transf.* **53** (5-6), 990–996.
- SBRAGAGLIA, MAURO, BENZI, ROBERTO, BIFERALE, LUCA, CHEN, HUDONG, SHAN, XIAOWEN & SUCCI, SAURO 2009 Lattice Boltzmann method with self-consistent thermo-hydrodynamic equilibria. *J. Fluid Mech.* **628**, 299.
- SHAN, XIAOWEN 2016 The mathematical structure of the lattices of the lattice Boltzmann method. *J. Comput. Sci.* **17**, 475–481.
- SHAN, XIAOWEN & CHEN, HUDONG 1993 Lattice Boltzmann model for simulating flows with multiple phases and components. *Phys. Rev. E* **47** (3), 1815–1819.
- SHAN, XIAOWEN & HE, XIAOYI 1998 Discretization of the Velocity Space in the Solution of the Boltzmann Equation. *Phys. Rev. Lett.* **80** (1), 65–68.
- SHAN, XIAOWEN, YUAN, XUE-FENG & CHEN, HUDONG 2006 Kinetic theory representation of hydrodynamics: a way beyond the Navier–Stokes equation. *J. Fluid Mech.* **550**, 413.
- SILVA, GONCALO & SEMIAO, VIRIATO 2012 First- and second-order forcing expansions in a lattice Boltzmann method reproducing isothermal hydrodynamics in artificial compressibility form. *J. Fluid Mech.* **698**, 282–303.
- YU, ZHAO & FAN, LIANG-SHIH 2009 An interaction potential based lattice Boltzmann method with adaptive mesh refinement (AMR) for two-phase flow simulation. *J. Comput. Phys.* **228** (17), 6456–6478.